

Climate sensitivity and the direct effect of carbon dioxide in a limited-area cloud-resolving model

DAVID M. ROMPS*

Department of Earth and Planetary Science, University of California, Berkeley, California, USA Climate and Ecosystem Sciences Division, Lawrence Berkeley National Laboratory, Berkeley, California, USA

ABSTRACT

Even in a small domain, it can be prohibitively expensive to run cloud-resolving greenhouse-gas warming experiments due to the long equilibration time. Here, a technique is introduced that reduces the computational cost of these experiments by an order of magnitude: instead of fixing the carbon-dioxide concentration and equilibrating the sea-surface temperature (SST), this technique fixes the SST and equilibrates the carbon-dioxide concentration. Using this approach in a cloud-resolving model of radiative-convective equilibrium (RCE), the equilibrated SST is obtained as a continuous function of carbon-dioxide concentrations spanning 1 ppmv to nearly 10,000 ppmv, revealing a dramatic increase in equilibrium climate sensitivity (ECS) at higher temperatures. This increase in ECS is due to both an increase in forcing and a decrease in the feedback parameter. In addition, the technique is used to obtain the direct effects of carbon dioxide, i.e., the rapid adjustments, over a wide range of SSTs. Overall, the direct effect of carbon dioxide offsets a quarter of the increase in precipitation from warming, reduces the shallow cloud fraction by a small amount, and has no impact on convective available potential energy (CAPE).

1. Introduction

One-dimensional (1D) models of radiative-convective equilibrium (RCE) have played an important role in our understanding of Earth's equilibrium climate sensitivity (Schlesinger 1986) from the early days of Manabe and Wetherald (1967) through to the recent work of (Kluft et al. 2019). Over the past two decades, it has become possible to replace those 1D

*Corresponding author address: David M. Romps, 307 McCone Hall, University of California, Berkeley, CA
E-mail: romps@berkeley.edu

models with 2D or 3D cloud-resolving models (CRMs), allowing for a more realistic treatment of clouds and convection. Unfortunately, the use of CRMs to study the response of RCE to altered CO_2 has been limited to only a handful of studies (Bretherton 2007; Romps 2011; Khairoutdinov and Yang 2013; Bretherton et al. 2014; Singh and O’Gorman 2015; Romps 2019), likely due to 1. the high computational cost of CRMs and 2. the multiple years required to fully equilibrate to a new concentration of CO_2 (Cronin and Emanuel 2013). To help overcome these barriers, this paper describes a technique that accelerates by a factor of 30 the equilibration of sea-surface temperature (SST) and CO_2 in small-area cloud-resolving simulations.

This $30\times$ speedup is relative to a simulation in which the slab ocean has negligible thickness (e.g., $\ll 1$ meter); this is often called a swamp ocean. Compared to simulations with a thick (e.g., $\gtrsim 1$ -meter) slab ocean, the speedup obtained with this technique is even greater than a factor of 30. Although the focus here is on CO_2 , this technique can be applied to the study of any radiative forcing, be it from variations in some other greenhouse gas or in the concentration of aerosols as in Khairoutdinov and Yang (2013). And, while we will study only standard small-domain CRM simulations of RCE here, the technique is equally applicable to any other model with a surface that is effectively 0D (e.g., a slab ocean with an infinite horizontal conductivity). Furthermore, as will be discussed in section 8, it should be possible to further extend the method to global climate models with a slab ocean.

But, again, the focus here is on CO_2 -induced warming in cloud-resolving simulations of RCE, and the great benefit of a technique for rapid equilibration is that it makes it computationally feasible to run many simulations. This has implications for the study of equilibrium climate sensitivity (ECS) and the direct effects of CO_2 .

With regards to ECS, global climate models (GCMs) exhibit a curious behavior: when run to high combinations of temperature and CO_2 , their ECS is found to have a pronounced maximum at SSTs in the range of 300-320 K (Russell et al. 2013; Wolf et al. 2018). But, since GCMs are expensive to run, the existing studies have included only about three simulations within that 20-K temperature range, giving ECS as only a coarsely resolved function of SST. Furthermore, it has been argued that the peak in ECS is caused by cloud feedbacks (Popp et al. 2016; Wolf et al. 2018), which motivates studying the phenomenon with cloud-resolving models. Here, the acceleration technique allows the ECS to be calculated in RCE as a smooth function of SST (with 1-K intervals) using cloud-resolving simulations.

In the study of the direct effects of carbon dioxide, global climate models have been used to quantify the rapid adjustment of clouds to a sudden change in CO_2 . This is typically done with a small handful of GCM experiments that simulate the effect of a sudden doubling or quadrupling of CO_2 (Gregory and Webb 2008; Andrews and Forster 2008; Colman and McAvaney 2011; Wyant et al. 2012; Zelinka et al. 2013; Kamae and Watanabe 2013). To get a fuller picture, at least in the context of RCE, the acceleration technique allows the direct effect to be explored over a wide range of SSTs and CO_2 concentrations in a CRM, where clouds are resolved rather than parameterized. This provides a bird’s-eye view of the direct effects of CO_2 relative to the effects of the resulting warming.

In the following sections, we will derive the relevant equilibration timescales (section 2), introduce the technique for rapidly approaching equilibration between the atmosphere, ocean, and CO₂ (section 3), and describe the cloud-resolving simulations to test the technique (section 4). Thanks to the speedup facilitated by the equilibration technique, 36 simulations are used to explore CO₂ concentrations ranging from below 1 ppmv to nearly 10,000 ppmv (section 5). Those simulations reveal an ECS that peaks prominently at warm temperatures (section 6). An additional set of simulations are then used to explore the direct effect of CO₂ on temperature, humidity, clouds, tropopause height, convective available potential energy (CAPE), and precipitation rate (section 7).

2. Timescales

Let us derive the time it takes for an atmosphere to equilibrate to a new RCE state in two different scenarios: a) an atmosphere over a zero-heat-capacity ocean (i.e., a slab ocean of infinitesimal thickness) being subjected to a sudden change in the top-of-atmosphere (TOA) forcing (say, from a sudden change in the concentration of CO₂), and b) an atmosphere over an infinite-heat-capacity ocean (i.e., an ocean with a fixed temperature) being subjected to a sudden change in its sea-surface temperature (SST). These timescales were derived by Cronin and Emanuel (2013) by solving an eigenvalue problem and then approximating the results. Here, we take shortcuts to the answers and relegate some of the details to the appendix.

a. An ocean with zero heat capacity

Consider an atmosphere over a slab ocean so thin that its heat capacity can be ignored. The response of the atmosphere to perturbations (denoted by Δ) in either the TOA radiative forcing F or near-surface air temperature T_a can be described as

$$C_a \frac{d\Delta T_a}{dt} = \Delta F + \lambda \Delta T_a, \quad (1)$$

where $\lambda \approx -1.5 \text{ W m}^{-2} \text{ K}^{-1}$ is the net feedback parameter for the ocean-atmosphere system¹ and C_a is the atmosphere's effective heat capacity. If ΔF is constant in time, then this can be solved to find

$$\Delta T_a = \frac{\Delta F}{|\lambda|} (1 - e^{-|\lambda|t/C_a}). \quad (2)$$

From this solution, we see that ΔT_a asymptotes to its equilibrated value of $\Delta F/|\lambda|$ with an e-folding timescale of $C_a/|\lambda|$. As derived in the appendix, C_a is about $2 \times 10^7 \text{ J m}^{-2} \text{ K}^{-1}$. Therefore, $C_a/|\lambda|$ equals about 150 days. Note that this is the equilibration timescale for an ocean of zero thickness. Each meter of slab ocean would add an additional 30 days to the timescale.

¹The value of $-1.5 \text{ W m}^{-2} \text{ K}^{-1}$ is the difference in equilibrated net upwelling TOA radiation for the FixC simulation at 320 K minus the FixC simulation at 285 K, divided by 35 K.

b. An ocean with infinite heat capacity

Consider an atmosphere over an ocean with an infinite heat capacity. In this case, the TOA radiative forcing is practically irrelevant because the tropospheric temperature is controlled by the fixed SST T_s . In the case of a zero-heat-capacity ocean, we were able to ignore the surface fluxes and write the prognostic equation for T_a in terms of TOA fluxes. With an infinite-heat-capacity ocean, we can ignore the TOA fluxes and write the prognostic equation for T_a in terms of surface fluxes. As shown in the appendix, this can be written as

$$C_a \frac{d}{dt} \Delta T_a = \chi \Delta(T_s - T_a), \quad (3)$$

where $\chi \approx 40 \text{ W m}^{-2} \text{ K}^{-1}$, encompassing sensible, latent, and radiative fluxes for typical tropical conditions. This tells us that any initial temperature perturbation in T_s will cause the air-sea temperature difference ($T_s - T_a$) to be driven back to its original value. If ΔT_s is constant in time, then this can be solved to find

$$\Delta T_a = \Delta T_s (1 - e^{-xt/C_a}) . \quad (4)$$

From this solution, we see that the air temperature perturbation is driven to its equilibrium value of ΔT_s with an e-folding timescale of C_a/χ .

Note that equation (4) is identical to (2) except that $\Delta F/|\lambda|$ has been replaced with ΔT_s and $|\lambda|$ (the magnitude of the atmosphere-ocean feedback parameter) has been replaced with χ (the surface enthalpy flux enhancement parameter). Since $|\lambda| \approx 1.5 \text{ W m}^{-2} \text{ K}^{-1}$ and $\chi \approx 40 \text{ W m}^{-2} \text{ K}^{-1}$, the timescale for equilibrating to a change in SST is about 30-times smaller than the timescale for equilibrating to a change in TOA radiative forcing. Instead of five months, the fixed-SST equilibration timescale is five days.

We see that these two equilibration timescales are very different. If we are interested in studying greenhouse-gas warming in RCE, we may wish to take advantage of the much shorter 5-day equilibration timescale rather than the long 5-month equilibration timescale. That is the objective of the next section.

3. The equilibration technique

The traditional method for equilibrating the atmosphere, ocean, and CO_2 is to fix the desired CO_2 concentration and let the atmosphere and ocean evolve until they equilibrate. This is accomplished by running the atmosphere over a slab ocean that obeys a simple prognostic equation relating its temperature tendency to the surface enthalpy-flux imbalance. That approach takes hundreds of days to equilibrate for the reason described in section 2a.

To take advantage of the much faster equilibration described in section 2b, we describe here a different approach. Rather than fixing the CO_2 concentration and evolving a prognostic equation for the SST, we will fix the SST and evolve a prognostic equation for the CO_2 concentration. The two methods are compared in Figure 1. For example, imagine we are interested in obtaining the ECS as a function of T_s . To obtain this, we can run a set of simulations, each with a different T_s , and let them equilibrate their atmosphere and their

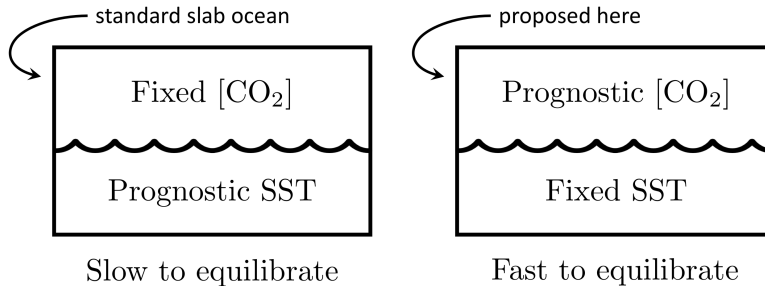


FIG. 1. (left) Standard slab-ocean simulations fix the CO_2 concentration and let the SST vary naturally according to its heat budget. This approach takes years of model time to equilibrate. (right) The technique proposed here is to fix the SST and let the CO_2 vary in a way that closes the TOA energy budget. This approach takes about one month of model time to equilibrate.

CO_2 concentration G . With the resulting pairs of T_s and G , we can then construct, by interpolation, the functions $T_s(G)$ and $G(T_s)$. The ECS, as a function of T_s , would then be given by

$$\text{ECS}(T_s) = T_s [2 \times G(T_s)] - T_s. \quad (5)$$

Let us derive the prognostic equation that G should obey in our simulations. A change in the net TOA downwelling radiative flux dN is related to a change in carbon-dioxide concentration dG as

$$dN = A d \log(G), \quad (6)$$

where A is often taken to be 5.35 W m^{-2} . Consider a situation in which the equilibrium net TOA downwelling radiative flux (equal to the applied ocean heat sink) is N_0 and the current value is N . Through a manipulation of the carbon-dioxide concentration, we wish to adjust N to N_0 on an e-folding timescale τ . In other words, we wish to implement controls on G that add a tendency to N equal to

$$\left. \frac{dN}{dt} \right|_{\text{due to } dG/dt} = \frac{N_0 - N}{\tau}. \quad (7)$$

Substituting dN from equation (6) into equation (7), we get

$$\frac{d}{dt} \log(G) = \frac{N_0 - N}{A\tau}. \quad (8)$$

To implement this, the timescale τ must be chosen with some care. It is tempting to choose an arbitrarily small value, but that would cause the CO_2 concentration to make large excursions in response to temporary TOA flux variations (due, e.g., to growing and shrinking cloud anvils). Here, we simply choose $\tau = 1$ week so that it is in the same ballpark as C_a/χ .

4. Simulations

To evaluate this equilibration technique and to employ it in a study of the direct effects of CO_2 , we will use three different sets of simulations, which we will refer to as SlabO, ProgC, and FixC. The SlabO simulations are standard slab-ocean simulations of the type depicted on the left in Figure 1; these are run with three different CO_2 concentrations. The

ProgC simulations use fixed SSTs and equation (8) to prognose CO₂, as depicted on the right in Figure 1; there are 36 of these simulations spanning SST values from 285 K to 320 K in 1-K increments. The FixC simulations use fixed SSTs (again, 36 simulations covering 36 SSTs) and a CO₂ concentration that is set to 280 ppmv; these are the “fixed-carbon” warming experiments most often performed with cloud-resolving models. These three sets of simulations are summarized in Table 1.

The cloud-resolving model used here is Das Atmosphärische Modell (DAM; Romps 2008), which has a finite-volume and fully compressible dynamical core coupled to a six-class single-mode microphysics scheme (Lin et al. 1983; Lord et al. 1984; Krueger et al. 1995) and the Rapid Radiative Transfer Model for General Circulation Models (RRTMG; Clough et al. 2005; Iacono et al. 2008) to represent shortwave and longwave radiation. In DAM, no explicit diffusion is added to the numerical diffusion already generated by the third-order advection scheme. The total solar irradiance and solar zenith angle are held fixed throughout the simulations. The cosine of the solar zenith angle θ is set to the insolation-weighted – i.e., $\cos(\theta)$ -weighted – average of $\cos(\theta)$ during the diurnal cycle at the equator on January 1 (Romps 2011). This gives a zenith angle of 43.75 degrees; this would be 43.91 degrees on the equator at the solstice, and both of these are similar to the value of $\arccos(2/3) \approx 48$ degrees that would be appropriate for a global average (Cronin 2014). Using a total solar irradiance (TSI) of 1366 W m^{-2} (somewhat higher than the modern estimate of 1361 W m^{-2} ; Kopp 2016), the daily averaged insolation at the equator on January 1 is 413.3 W m^{-2} . The model’s TSI is set to that mean insolation (413.3 W m^{-2}) divided by $\cos(43.75^\circ)$, which equals 572.1 W m^{-2} . In similar configurations, DAM has been shown to broadly match conditions observed in the tropics, although it produces a higher CAPE and relative humidity (Romps 2011) and a lower cloud fraction (Seeley et al. 2019).

By volume, N₂ and O₂ are set to 79% and 21% of dry air, respectively, and those percentages are then reduced proportionately to accommodate the specified concentration of CO₂. The radiation scheme sees nitrogen, oxygen, carbon dioxide, water vapor, cloud drops, and cloud ice. Ozone is excluded from these runs because DAM does not have a chemistry module that would allow the ozone profile to evolve in a mechanistic way in the warming experiments. Fortunately, stratospheric ozone has only a small impact on equilibrium climate sensitivity (Dacie et al. 2019).

All of the simulations have their domain-averaged horizontal wind damped to zero on a 1-hour timescale. Surface fluxes of mass, momentum, and energy are calculated using bulk-aerodynamic formulae with a fixed 5-m/s wind speed and a transfer coefficient of 1.5×10^{-3} . All domains have a model top at a height of 61 km. Unless specified otherwise, the model domain is square and 108-km wide; this domain is used for all of the SlabO, ProgC, and FixC simulations, and is small enough to avoid convective aggregation. The horizontal grid spacing is set to a uniform 1 km, and a stretched grid is used in the vertical with 134 levels whose spacing smoothly transitions from a uniform $\Delta z = 50 \text{ m}$ below an altitude of 500 m to a uniform $\Delta z = 500 \text{ m}$ between altitudes of 5 km and 48 km. The effect of the Brewer-Dobson circulation on water vapor is emulated by relaxing (on a five-day timescale) the

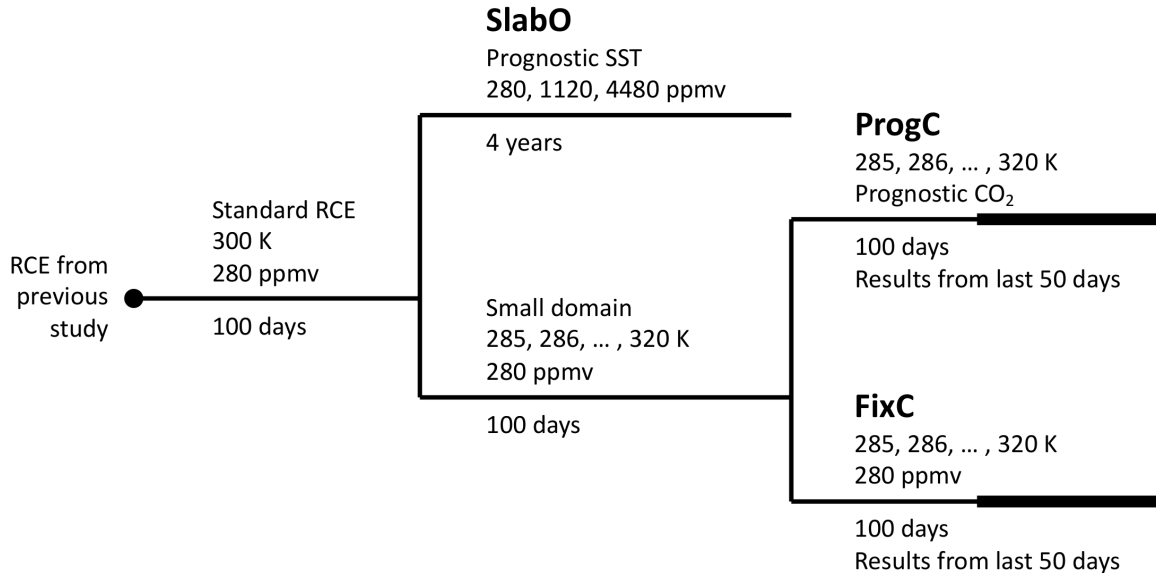


FIG. 2. Timeline indicating how each set of simulations is initialized. The thick solid lines denote the last 50 days of the ProgC and FixC simulations, over which quantities are averaged to obtain equilibrated values.

water-vapor mass fraction at each height in the stratosphere to the smaller of 1. the value at the tropopause (where there is zero net radiative cooling) and 2. the smallest value between the tropopause and that height.

The timeline of the simulations is shown in Figure 2. The first step is to identify the appropriate TOA flux imbalance, which will be applied as a cooling of the ocean for the SlabO simulations and also used as the value of N_0 in equation (8) for the ProgC simulations. To this end, the first cloud-resolving simulation (labeled “Standard RCE” in Figure 2) is run over a 300-K ocean with a CO₂ concentration of 280 ppmv. This simulation is restarted from a similar RCE profile, but is run for 100 days to ensure equilibration. Because this is a fixed-SST run, there is an imbalance in the enthalpy fluxes at the top of the atmosphere (TOA) and at the ocean surface. Once equilibrated, those imbalances are equal because there can be no net convergence of energy into the atmosphere. Averaging over the last 50 days of the simulation, the TOA net downwelling radiative flux is found to be 112 W m^{-2} . As noted by Romps (2011), this matches the $\sim 100 \text{ W m}^{-2}$ of net downwelling radiative flux observed at the top of the atmosphere over the western Pacific warm pool (Tian et al. 2001).

The SlabO simulations are restarted directly from the end of that “Standard RCE” simulation. The three SlabO simulations are run with $1\times$, $4\times$, and $16\times$ the original CO₂ concentration (i.e., 280 ppmv, 1120 ppmv, and 4480 ppmv). The slab ocean is given a depth of 20 cm, is initialized to 300 K, and is cooled at a rate of 112 W m^{-2} to guarantee that the 280-ppmv simulation equilibrates to an SST of 300 K. Each SlabO simulation is run for four years.

Before starting the ProgC and FixC simulations, a set of 36 simulations are run on a small 16-km-wide square domain with SSTs ranging from 285 to 320 K in 1-K increments.

Name	SST	CO ₂
SlabO	prognostic	280, 1120, & 4480 ppmv
ProgC	280, 281, . . . , 320 K	prognostic
FixC	280, 281, . . . , 320 K	280 ppmv

TABLE 1. The three types of simulations: slab ocean (SlabO), prognostic CO₂ (ProgC), and CO₂ fixed at 280 ppmv (FixC).

These simulations are labeled “Small domain” in Figure 2, are restarted from the “Standard RCE” simulation, and are run for 100 days. The point of these small-domain simulations is to bring the atmosphere to rough equilibration with its new SST in a computationally inexpensive manner. After 100 days of those small-domain simulations, each of the ProgC and FixC simulations are restarted from the small-domain simulations with the matching SST. ProgC uses equation (8) with $N_0 = 112 \text{ W m}^{-2}$ and $\tau = 1$ week. FixC uses a fixed CO₂ concentration of 280 ppmv. The ProgC and FixC simulations are run for 100 days and equilibrated properties are obtained by averaging over the last 50 days.

5. Results

The bottom panel of Figure 3 shows how the SlabO simulations approach equilibrium. The 280-ppmv slab-ocean simulation does nothing interesting, as expected, because it is restarted with the same SST and CO₂ concentration as the already equilibrated RCE simulation. The $4\times\text{CO}_2$ (1120 ppmv) simulation reaches its equilibrated SST in about 3 years, while the $16\times\text{CO}_2$ (4480 ppmv) simulation is still not equilibrated after 4 years.

In contrast, the ProgC simulations equilibrate in a couple months. The top and middle panels of Figure 3 show the time series of surface-air temperature and CO₂ concentration, respectively, for these simulations. Although the simulations are run for a total of 200 days (split into 100 days of the fixed-CO₂ on a small domain followed by 100 days of ProgC on the standard domain), that is more time than is needed to reach equilibration. In the first span of 100 days, the simulations fully equilibrate to the new SST in about 30 days, which is as expected: this is several multiples of the 5-day e-folding time calculated in section 2b. In the second span of 100 days, the simulations equilibrate their TOA flux in about 30 days: this is a few multiples of the 1-week CO₂ adjustment timescale used in equation (8).

As a sanity check, we can confirm that the ProgC simulations have the desired net TOA flux. Figure 4 plots the time series of each simulation’s net TOA downwelling radiation anomaly (i.e., net downwelling TOA minus 112 W m^{-2}), which are offset in the vertical so that each time series can be seen. Each thin horizontal line corresponds to zero TOA anomaly for the SST value that it intercepts on the ordinate. Within a month of switching to the prognostic equation for CO₂, the simulations have adjusted their TOA flux anomaly to zero. Although this is a useful sanity check, it is important to note the TOA flux anomaly is forced to go to zero by equation (8) on whatever timescale we choose. Had we chosen a 1-minute timescale, this TOA flux anomaly would have gone to zero within a few minutes from the 100-day mark. (Recall that we choose a 1-week timescale to prevent the CO₂ concentration from

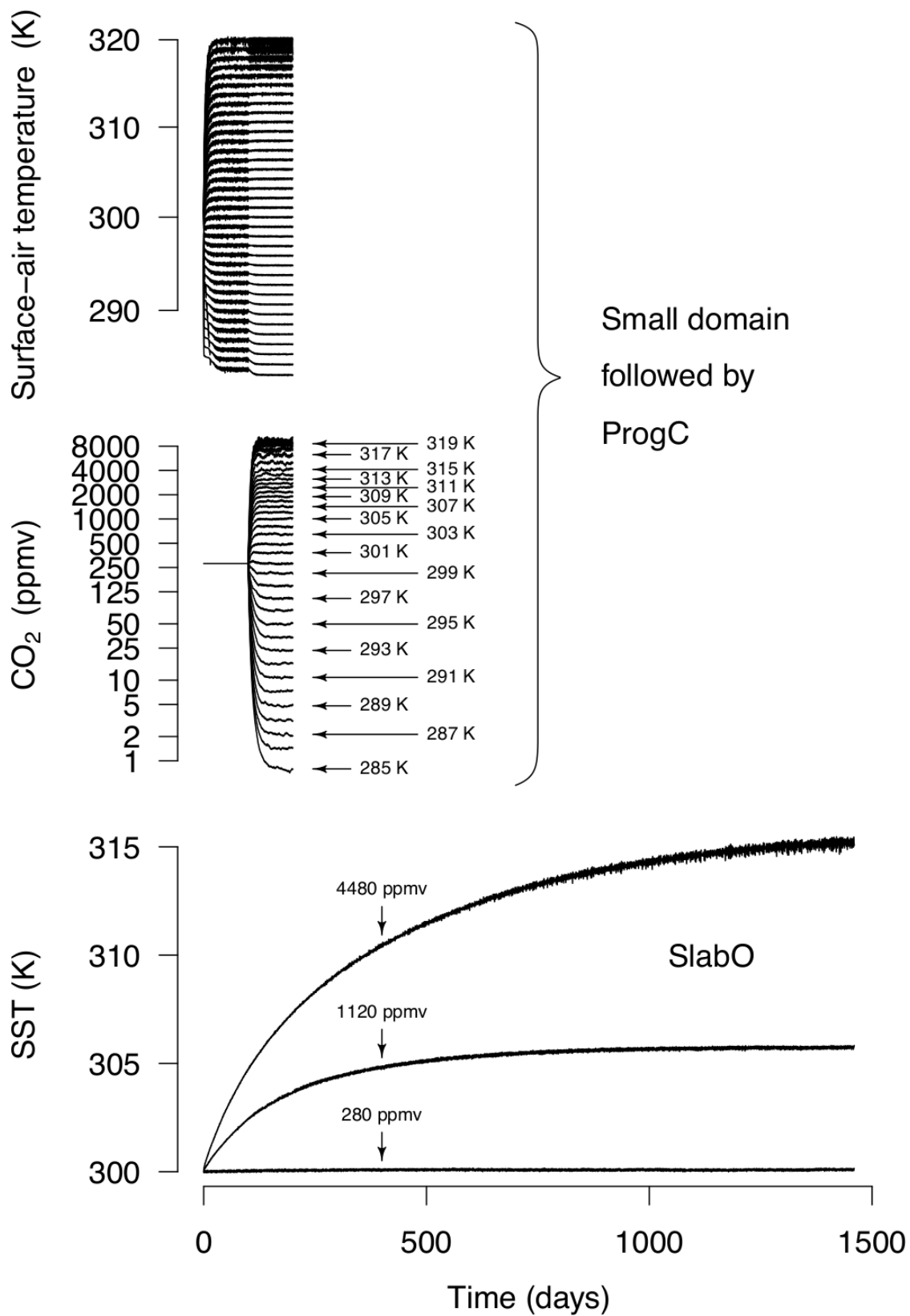


FIG. 3. (top row) Time series of surface-air temperature for the small-domain simulations (first 100 days) followed by the ProgC simulations (next 100 days). (middle row) Same, but for CO₂. (bottom row) Time series of SST for the SlabO simulations.

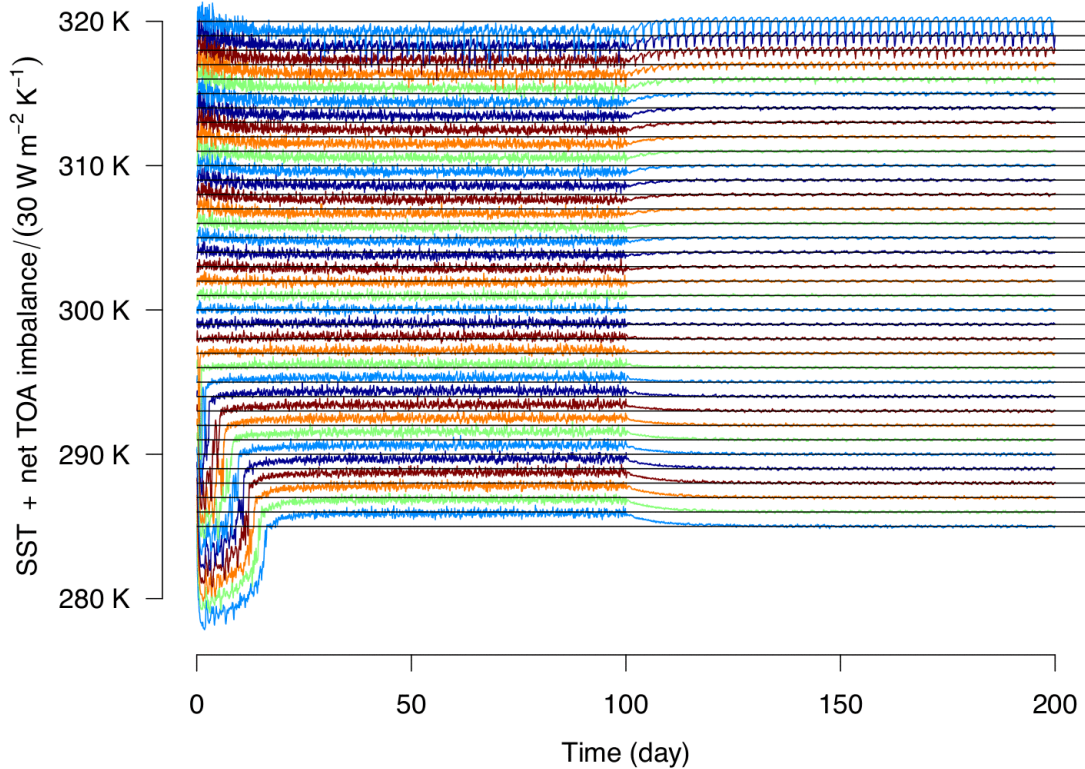


FIG. 4. Time series of net downwelling TOA radiative-flux imbalance (TOA downwelling flux minus 112 W m^{-2}) for the experiments using fixed-SST/fixe-CO₂ on the small domain for the first 100 days and fixed-SST/prognostic-CO₂ ProgC simulations for the next 100 days. The time series are shifted in the vertical by dividing the TOA imbalance by $30 \text{ W m}^{-2} \text{ K}^{-1}$ and adding the SST; therefore, every 1 K of displacement on the vertical axis corresponds to 30 W m^{-2} of net TOA imbalance. The thin horizontal lines mark the 36 SST values, which correspond to zero TOA imbalance.

undergoing wild swings.) The more compelling evidence that a simulation has equilibrated is that its CO₂ concentration has reached a steady value. As we saw in Figure 3, this occurs after about one month, implying that any remaining stratospheric temperature adjustment that continues beyond a month (on the order of 1–10 K) has no consequential impact on the atmosphere’s energy balance.

Since the ProgC simulations equilibrate after 30 days, we can average the CO₂ concentration over the last 50 days of the 100-day simulations to get the equilibrated CO₂ concentrations (denoted by G). This gives us 36 pairs of T_s and G (one pair for each T_s from 285 K to 320 K in 1-K increments). We can linearly interpolate between these 36 pairs to produce $T_s(G)$ as a piecewise-linear function. This is plotted in Figure 5. Note that the low computational cost of these simulations – made possible by the fixed-SST/prognostic-CO₂ methodology – has allowed us to evaluate this function at 1-K intervals in a cloud-resolving model.

To confirm that the ProgC simulations are giving the correct $T_s(G)$ relationship, we can compare them to the SlabO simulations. Since the $16\times\text{CO}_2$ simulation has not fully equilibrated after four years, Figure 6 shows the Gregory plots (Gregory et al. 2004) for each

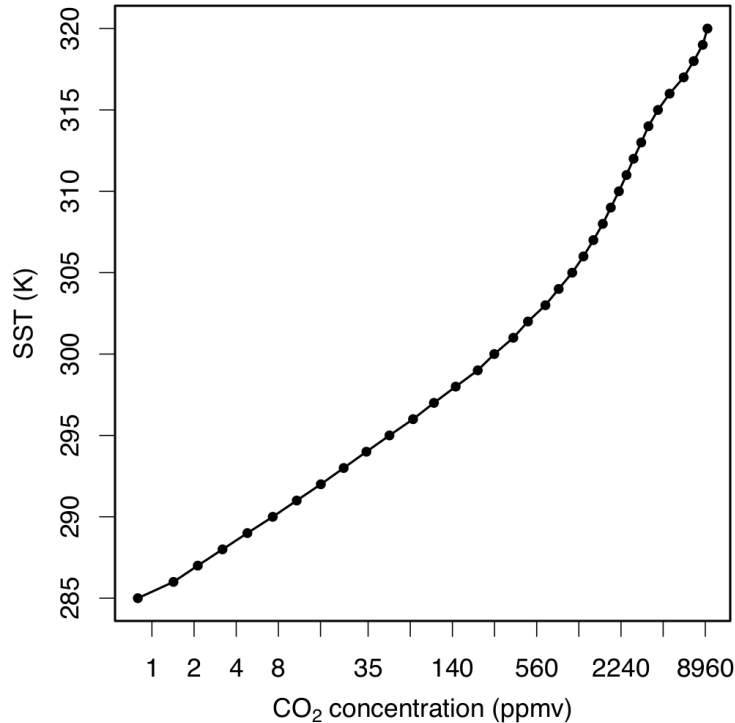


FIG. 5. The function $SST(CO_2)$ created by linearly interpolating the 36 equilibrated fixed-SST/prognostic- CO_2 simulations, which are plotted as black dots.

of the runs. Each grey dot represents an hourly average of the slab-ocean simulation, and the solid black lines follow the monthly average. The diamonds show the predictions from the $T_s(G)$ function of Figure 5, derived from the ProgC simulations. Regardless of how one fits a line to the SlabO data (e.g., over the last 6 months, the last 24 hours, or any length of time in between), the Gregory-plot data predict equilibrated SSTs that are within 0.1 to 0.3 K of the values obtained from Figure 5.

6. Equilibrium climate sensitivity

Since Figure 5 uses a logarithmic axis for the CO_2 concentration, a constant equilibrium climate sensitivity (ECS; the change in SST per doubling of CO_2) would correspond to a straight line in this plot. We see departures from this behavior at very low CO_2 concentrations (at and below 1 ppmv) and at concentrations above 280 ppmv. The departure from a constant ECS at low CO_2 concentrations is due to the fact that CO_2 loses its efficacy as a greenhouse gas at concentrations just below 1 ppmv. If the curve were continued to the left, it would approximate a horizontal line at an SST of around 284-285 K.

At high temperatures and CO_2 concentrations, there is a remarkable increase in the ECS, which is caused by variations in both the CO_2 forcing and the feedback parameter. The left panel of Figure 7 shows the instantaneous top-of-atmosphere radiative forcing from doubling

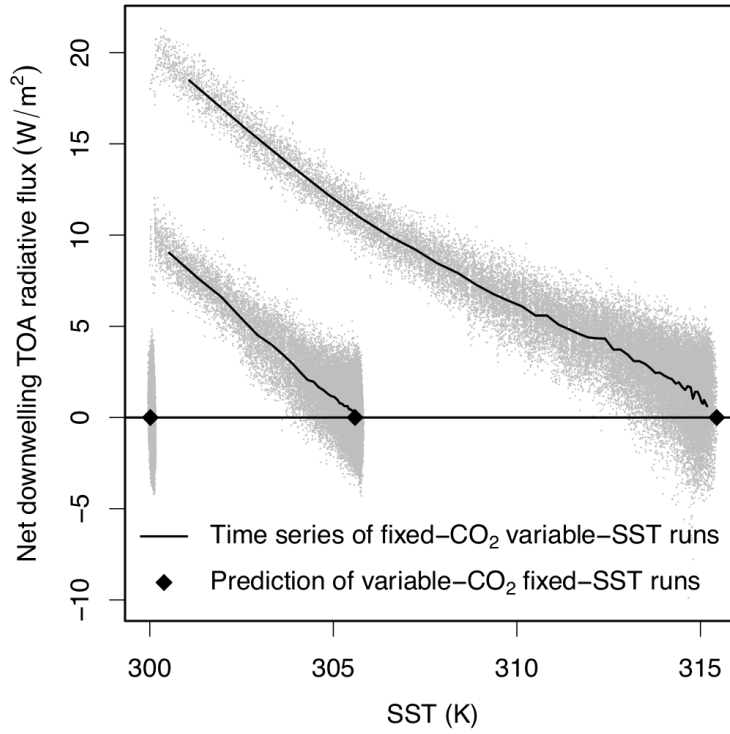


FIG. 6. Gregory plot of the three slab-ocean simulations with $1\times$, $4\times$, and $16\times$ the reference CO_2 concentration of 280 ppmv. The grey dots are hourly averages and black curves are monthly averages. The diamonds mark the final SST predicted by the $\text{SST}(\text{CO}_2)$ curve in Figure 5.

CO_2 . We see that the radiative forcing increases from 0 W m^{-2} at 0 ppmv, to about 4 W m^{-2} at 280 ppmv, to over 5 W m^{-2} at concentrations exceeding 1600 ppmv. This is consistent with studies using global climate models (Hansen et al. 2005; Colman and McAvaney 2009; Caballero and Huber 2013; Wolf et al. 2018) and a simple RCE model (Kluft et al. 2019), which have all found that a doubling of CO_2 causes greater radiative forcing at higher CO_2 concentrations. As we can confirm by comparing to the FixC runs, this variation in forcing is due to the change in the CO_2 concentration, not the warming.

The middle panel of Figure 7 shows the inverse magnitude of the feedback parameter, which is often referred to as the climate sensitivity (with units of $\text{K W}^{-1} \text{ m}^2$, not to be confused with the equilibrium climate sensitivity). Here, the feedback parameter is defined as the ECS, as defined by equation (5), divided by the instantaneous top-of-atmosphere doubled- CO_2 forcing. We see that the climate sensitivity peaks around 310 K, matching the location of the peak at around 300-320 K found in global climate models (Leconte et al. 2013; Wolf and Toon 2015; Popp et al. 2016; Wolf et al. 2018). Finally, the last panel shows the product of the forcing and the climate sensitivity, which is the ECS. The ECS exhibits a peak around 310 K, consistent with the behavior found in both a 1D model (Meraner et al. 2013) and global climate models (Russell et al. 2013; Wolf et al. 2018).

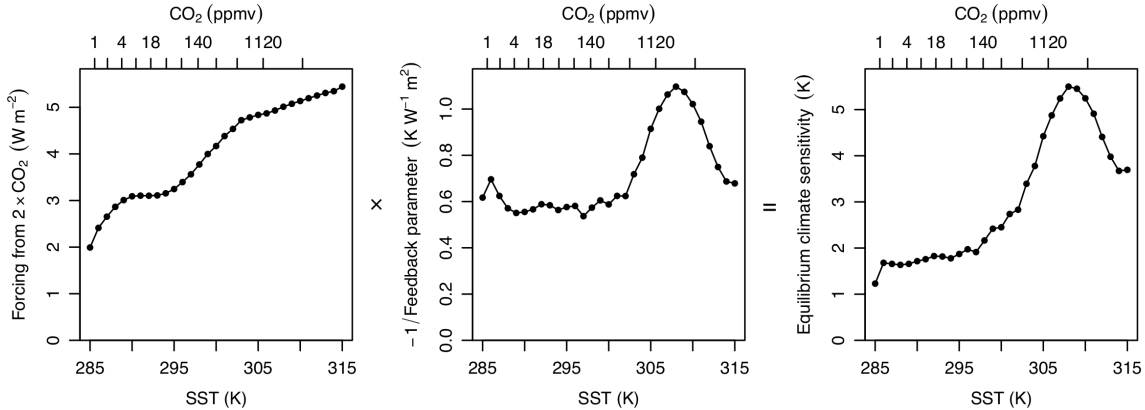


FIG. 7. As a function of SST, the (left) instantaneous top-of-atmosphere forcing from doubling the CO₂ concentration, (middle) inverse magnitude of the feedback parameter (a.k.a. the “climate sensitivity”), and (right) product of the two, which is the equilibrium climate sensitivity (ECS).

7. Direct effects of CO₂

When trying to achieve an equilibrated RCE with the desired TOA net radiative flux, we have seen that it is much faster, and just as accurate, to evolve the CO₂ concentration instead of the SST. But, when using RCE simulations to study greenhouse-gas warming, is it really necessary to enforce a constant net TOA flux? Why not hold the CO₂ concentration constant and simply step up the SST as has been done many times before in studies with both CRMs (e.g., Muller et al. 2011; Cronin and Wing 2017) and GCMs (e.g., Cess and Potter 1988)?

The simulations performed in that way (i.e., with varied SST, but constant CO₂) will have different values of the net TOA flux, but they may be adequate for answering many types of questions. Of course, if the goal is to accurately calculate the climate sensitivity, there is no substitute for equilibrating two or more simulations (with different CO₂ concentrations) to the same TOA flux. For everything else, however, the relevant question is whether the “direct effect” of CO₂ (i.e., the impact of varying CO₂ while holding SST fixed) matters for the phenomenon being studied (Sherwood et al. 2015; Kamae et al. 2015). The new equilibration technique allows us to explore the direct effects of CO₂ as continuous functions of surface temperature.

As a reminder, FixC is identical to ProgC, except that the CO₂ concentration is held fixed at 280 ppmv; therefore, a variable in ProgC minus the same variable in FixC is the direct effect of CO₂ on that variable. The four rows of Figure 8 show profiles of temperature, specific humidity, cloud fraction, and net radiative heating in the ProgC and FixC simulations (left and middle columns, respectively), along with their differences (right column). Each simulation is color-coded, ranging from the darkest blue at an SST of 285 K, through blue-green at 300 K, and up to the darkest red at 320 K. By eye, we see that the profiles in the left column (ProgC) are very similar to the profiles in the middle column (FixC). This tells us that the effect of warming on these four variables is much larger than the direct effect

of CO₂. (Note that the differences in the third column are plotted over a smaller range to make visible the relatively small direct effect.)

Although the direct effects of CO₂ are relatively small in magnitude, they are robust. Focusing on the right column of Figure 8, we see that an increase in CO₂ concentration (red colors; vice versa for blue) while holding SST fixed tends to: a) warm the troposphere, b) humidify the troposphere, c) decrease cloud cover (Gregory and Webb 2008; Andrews and Forster 2008; Colman and McAvaney 2011; Zelinka et al. 2013; Kamae and Watanabe 2013), and d) decrease radiative cooling (Newell and Doplick 1970), which will then cause a reduction in precipitation (Mitchell et al. 1987).

To quantify the relative impacts of the direct effect and the warming effect, we can calculate mean absolute changes for both of these. In particular, let us calculate the mean absolute change in temperature, specific humidity, cloud fraction, and radiative cooling over all SST values and from heights up to 12 km (which is in the troposphere for all SST values), once for the direct effect and once again for the warming effect. For X equal to one of temperature, specific humidity, cloud fraction, and radiative cooling, Figure 9 gives the value of

$$\frac{1}{35 \text{ K}} \int_{285 \text{ K}}^{320 \text{ K}} dT_s \frac{1}{12 \text{ km}} \int_{0 \text{ km}}^{12 \text{ km}} dz |\Delta X|, \quad (9)$$

where Δ is the difference either between ProgC and FixC (for the direct effect) or between FixC and FixC at 300 K (for the warming effect). We see that the warming effect is at least an order of magnitude larger than the direct effect for tropospheric temperature, specific humidity, and cloud fraction. For the radiative cooling, the magnitude of the direct effect is about one third that of the warming effect.

Although Figure 9 suggests that the changes in cloud cover from the direct effect are an order of magnitude smaller than from warming, changes calculated using equation (9) include vertical shifts in clouds that may not be as relevant to the atmosphere's energy balance as changes in the magnitudes of cloud-fraction maxima. To tease apart these two effects, we can track the changes in the location and areal fraction of the lower and upper peaks in cloudiness. The left panel of Figure 10 shows the profile of cloud fraction from the base simulation (300 K, 280 ppmv). The lower and upper peaks in cloudiness are identified as the maxima of quadratic fits to the three closest points, and they are marked in the left panel by colored lines. Those four colors correspond to the four other panels, which show their variations with SST in the (dashed) FixC and (solid) ProgC simulations. (The CO₂ axes are shown for the ProgC simulations; the FixC simulations all use 280 ppmv.) The dashed curves show how the clouds change in response to an altered SST. The solid curves show how the clouds change in response to both an altered SST and the altered CO₂ required to generate that SST in an energetically balanced way. Therefore, the difference between the dashed and solid curves is the direct effect of CO₂ on the clouds. Since the dashed and solid curves are nearly identical, we see that the direct effect is small. Nevertheless, there is a noticeable and consistent direct effect on the shallow-cumulus peak: an increase in CO₂

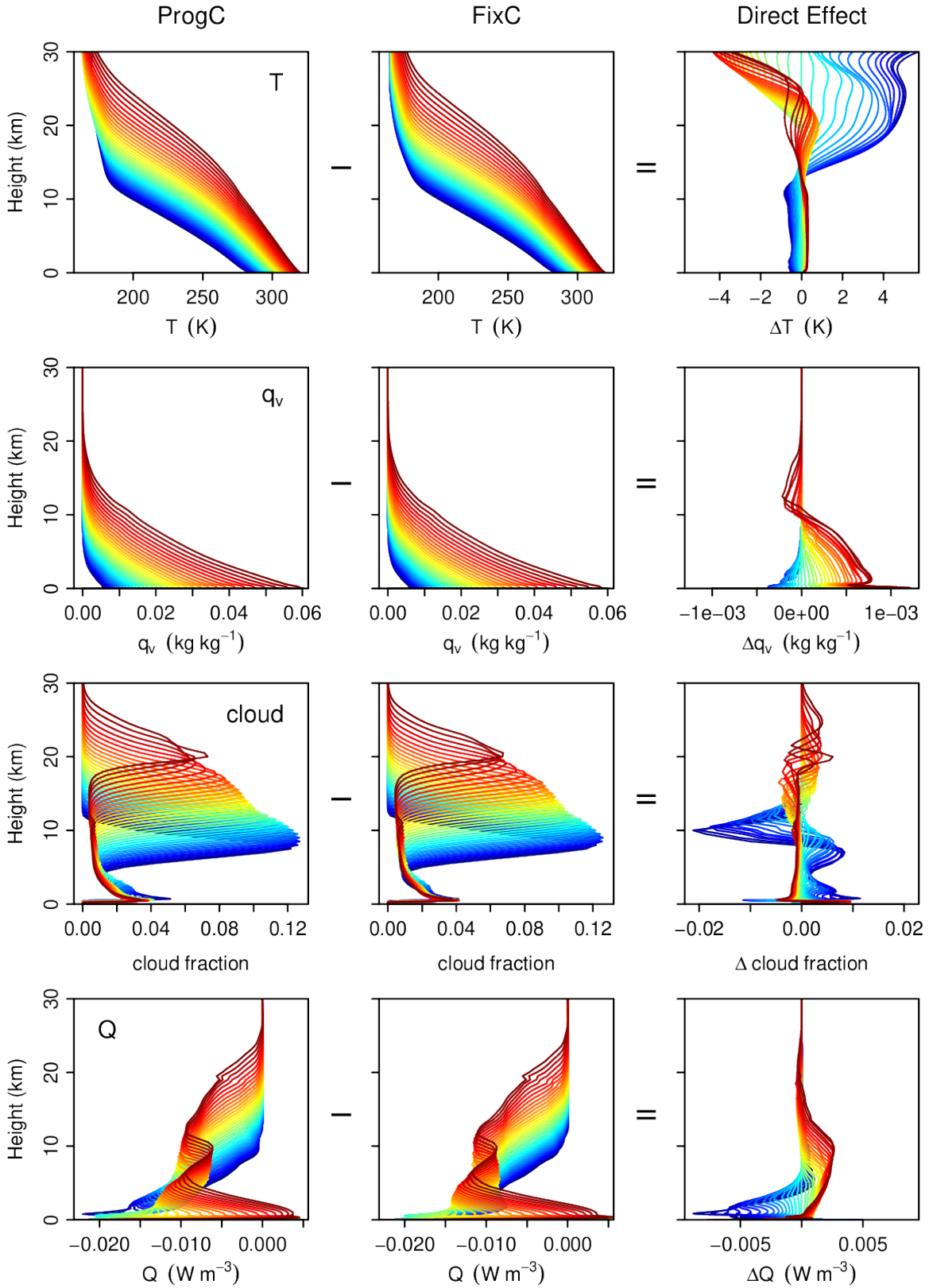


FIG. 8. Profiles of (top row) temperature, (second row) specific humidity, (third row) cloud fraction, and (bottom row) radiative heating in the (left column) ProgC and (middle column) FixC simulations. The simulations are color-coded from dark blue to dark red as the SST increases from 285 K to 320 K, as can be seen from where the temperature profiles intercept the abscissa. The right column shows the difference in the profiles between the ProgC and FixC simulations at the same SST; this is the direct effect of CO_2 becoming (red) higher and (blue) lower than 280 ppmv.

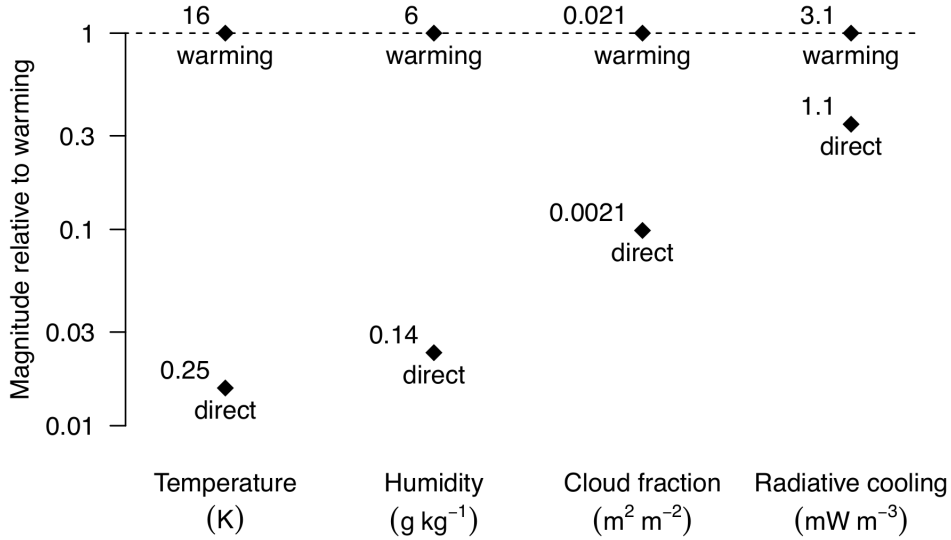


FIG. 9. The direct effect and warming effect, as calculated using expression (9) using the appropriate definition of Δ , for temperature, specific humidity, cloud fraction, and radiative cooling. The numbers next to each diamond give the values calculated by expression (9) and the position of the diamonds on the logarithmic ordinate illustrate the magnitude relative to the warming effect (e.g., for the direct effect on temperature, $0.25/16 = 0.016$).

tends to lower the height of the shallow clouds (consistent with Wyant et al. 2012; Kamae and Watanabe 2013; Andrews and Ringer 2014) and decrease their total area.

Despite the fact that RCE has no large-scale circulation (e.g., no subtropical stratus), the magnitude of the direct effect of CO_2 on shallow clouds found here in RCE is similar to what is seen in global climate models. Zelinka et al. (2013) studied the effect of quadrupling CO_2 while holding SSTs fixed in five climate models. Their Figure 7 shows the profiles of cloud fraction in the lower troposphere (averaged equatorward of 45° in regions of high lower-tropospheric stability) from the five models for two different experiments: one with climatological SSTs and one with climatological SSTs and quadrupled CO_2 . Extracting the data directly from the vector graphics and applying a quadratic fit to identify the location and value of the lower-tropospheric peak, the effect of quadrupling CO_2 is found to change the peak cloud cover by a fractional amount of +1, -7, -3, -1, and -1% for CanESM2, CCSM4, MIROC5, MRI-CGCM3, and HadGEM2-A, respectively. (Note that these are fractional changes in the cloud cover; e.g., for a cloud cover of 10%, a -1% fractional change means that the cloud cover becomes 9.9%.) The average fractional change in cloud cover among these five GCMs is -2% for a quadrupling of CO_2 . In the RCE simulations, we can calculate the fractional change in the peak in lower cloud cover from a quadrupling of CO_2 , and we can apportion that change to the warming (i.e., the change in SST) and the direct effect (i.e., the change in CO_2). This is accomplished by comparing three cases: the FixC simulation at 300 K and 280 ppmv, the ProgC simulations interpolated to 1120 ppmv (with a corresponding SST of 305.6 K), and FixC simulations (with 280 ppmv) interpolated to an SST of 305.6 K. The result is that the warming associated with a quadrupling of CO_2

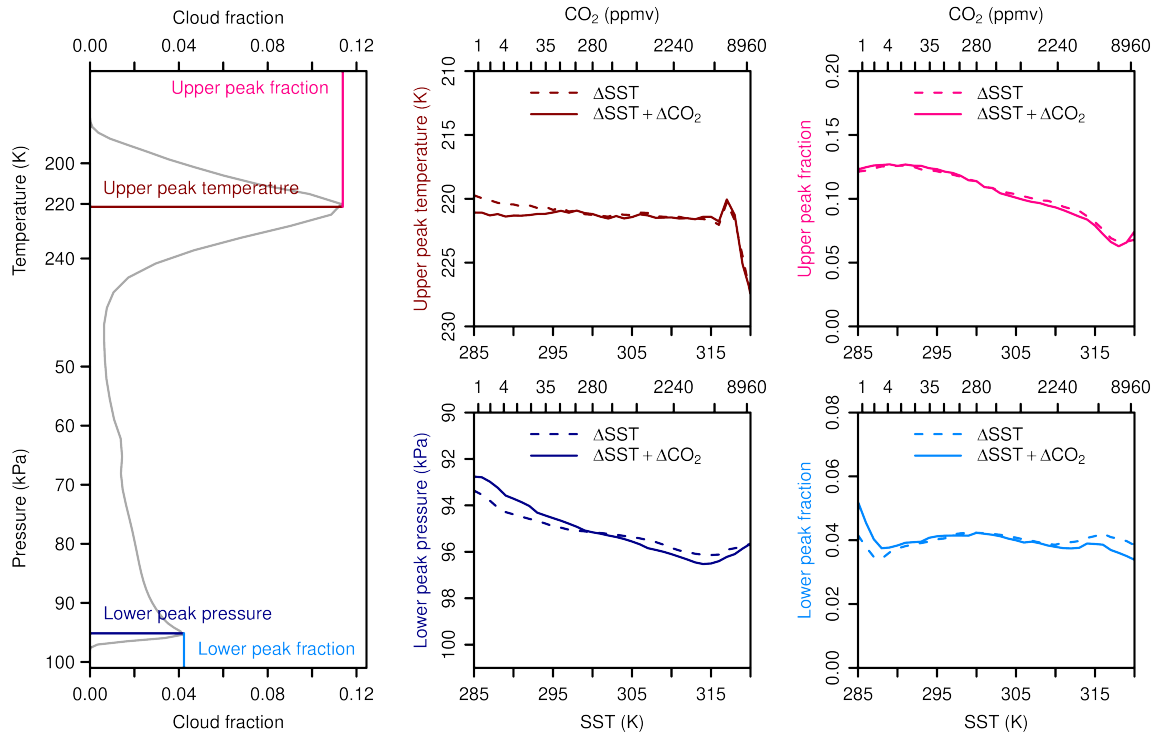


FIG. 10. (left column) The profile of cloud fraction in the base simulation with a 300-K ocean and a 280-ppmv CO₂ concentration. The cloud fractions and locations of the lower (cumulus) peak and the upper (anvil) peak are indicated by four different colors, which correspond to the colors used in the other panels. (middle top) Anvil temperature in the (dashed) FixC simulations and (solid) ProgC simulations as a function of SST (the CO₂ axis is for the ProgC simulations only; the FixC simulations all use 280 ppmv). (right top) Same, but for anvil cloud fraction. (middle bottom) Same, but for cumulus pressure. (right bottom) As in right top, but for cumulus cloud fraction.

leads to a -4% fractional change, while the direct effect of the quadrupled CO₂ generates an additional -2% fractional change, matching what is found in the data of Zelinka et al. (2013). Likewise, the large-eddy simulations of Wyant et al. (2012) also generated a -2% fractional change in low cloud cover in response to a quadrupling of CO₂.

Before we conclude, let us look at three more quantities – the tropopause height, CAPE, and the precipitation rate – to see if they are affected directly by CO₂. We might expect CO₂ to affect the tropopause height through its direct impact on the balance between shortwave O₃ heating and longwave CO₂ cooling. Recall, however, that there is no ozone in these simulations, so the stratosphere is relatively cold and relatively insensitive to CO₂. Indeed, Figure 11a shows that the tropopause height in these simulations is virtually unaffected by the CO₂ concentration. The tropopause is defined here as the height where the net radiative cooling is zero; due to convective cooling from overshooting updrafts, there is a layer of compensatory radiative heating atop the troposphere and, therefore, a well-defined height at which the net radiative cooling is exactly zero. In this panel and the others of Figure 11, there are two curves: one for the equilibrated-CO₂ simulations (solid) and one for the 280-

ppmv simulations (dashed). In Figure 11a, the two curves are nearly identical, indicating that the direct effect of CO_2 on the tropopause height is negligible in these simulations.

As for CAPE, recent work has shown that CAPE is set by the difference between the adiabatic lapse rate and the entraining lapse rate (Singh and O’Gorman 2013; Romps 2016; Seeley and Romps 2016). Given the entrainment rate and the temperature and humidity profiles, we can calculate these lapse rates and therefore, CAPE. We have already seen in Figure 9 that the direct effect of CO_2 on temperature and humidity is an order of magnitude less than the effect from sea-surface warming, so a natural hypothesis is that CAPE is not much affected directly by CO_2 . Figure 11b confirms this: CAPE as a function of SST is largely unaffected by variations in CO_2 .

Finally, let us consider the precipitation rate. Since the precipitation rate is closely pegged to the net radiative cooling of the troposphere, and since an addition of CO_2 reduces that cooling (as noted in the discussion of Figure 8), we know that a direct effect of CO_2 must be to cause a decrease in precipitation (Mitchell et al. 1987; O’Gorman et al. 2012). Figure 11c confirms such an effect, albeit a modest one. The FixC simulations (in which net upwelling TOA flux increases with SST) generate an average rate of precipitation increase of $3.0\% \text{ K}^{-1}$. The ProgC experiments (in which the net upwelling TOA flux is constant) generate an increase of $2.3\% \text{ K}^{-1}$, in line with GCMs subjected to CO_2 -induced warming (Held and Soden 2006; Lambert and Webb 2008; Stephens and Ellis 2008). We see that the direct effect cuts into the precipitation increase by about one quarter, which is consistent with the direct effect on radiative cooling being about a third as large as the warming effect, as seen in Figure 9.

8. Summary and Discussion

In section 2, we derived the timescales for an atmosphere and ocean to equilibrate under two scenarios: a zero-heat-capacity ocean and an infinite-heat-capacity ocean. In either case, the equilibration timescale is given by the heat capacity of the atmosphere divided by the sensitivity to temperature of an enthalpy flux. In the case of an ocean with zero heat capacity, the relevant flux is the net radiative flux at the top of the atmosphere, which has a weak sensitivity to the deviation of the near-surface air temperature from its equilibrium value ($\sim 1.5 \text{ W m}^{-2} \text{ K}^{-1}$). In the case of an ocean with infinite heat capacity, the relevant flux is the net enthalpy flux at the surface, which has a strong sensitivity to the deviation of the near-surface air temperature from its equilibrium value ($\sim 40 \text{ W m}^{-2} \text{ K}^{-1}$). By virtue of these different sensitivities, an atmosphere over a fixed sea-surface temperature will approach equilibrium with the SST about 30 times faster than an atmosphere over a thin slab ocean will approach a zero TOA flux anomaly.

This motivated the equilibration technique described in section 3, which reduces by $30\times$ the computational time required to conduct greenhouse-gas warming experiments in limited-area cloud-resolving models. The idea is to apply a fixed temperature increment to the surface and then allow both the atmosphere and the carbon-dioxide concentration to

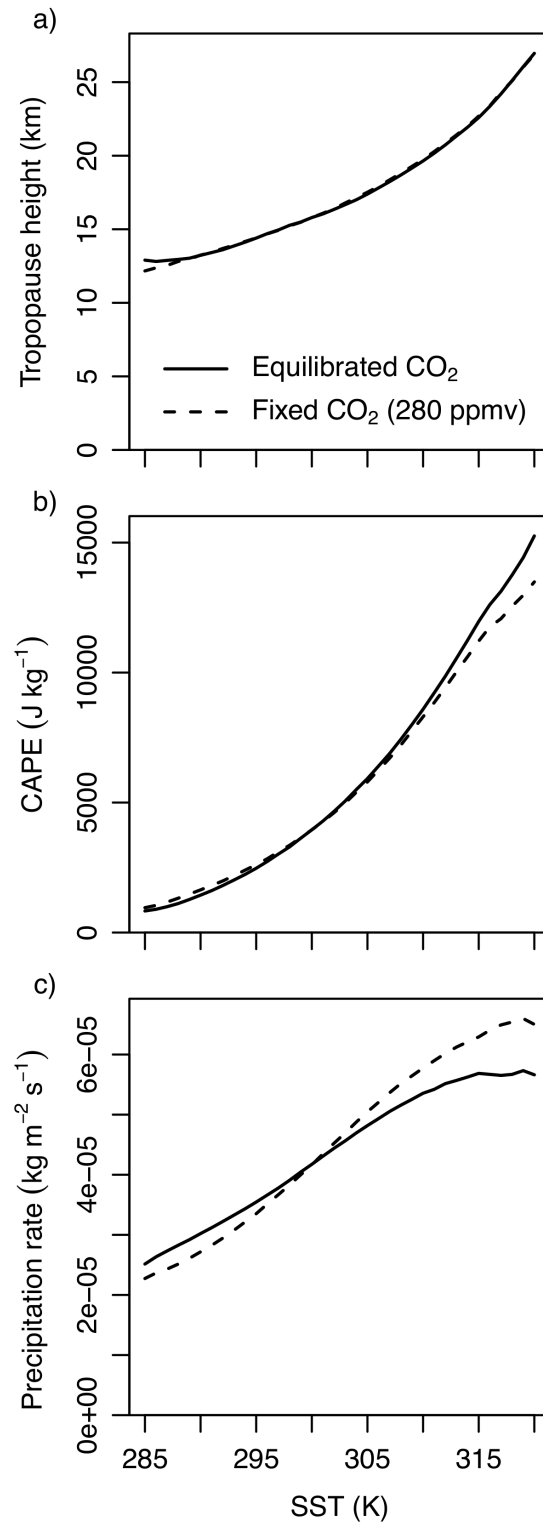


FIG. 11. (a) The tropopause height as a function of SST for (solid) simulations in which CO₂ is equilibrated and (dashed) simulations in which CO₂ is held constant at 280 ppmv. (b) Same, but for CAPE. (c) Same, but for the precipitation rate.

evolve prognostically. The equation used to evolve the CO₂ concentration is one that drives the net TOA radiative flux anomaly to zero on a reasonably short timescale, chosen here to be one week.

This technique was used in sections 4 and 5 to equilibrate a cloud-resolving model to 36 different concentrations of carbon dioxide. This produced the sea-surface temperature as a continuous function of the CO₂ concentration, as shown in Figure 5. This revealed a peak in the equilibrium climate sensitivity (ECS) at warmer temperatures as seen in the right panel of Figure 7. There are two contributions to this peak in ECS. The first is that the forcing from a doubling of CO₂ increases with the CO₂ concentration from 0 to over 5 W m⁻². The second is that the magnitude of the feedback parameter (climate sensitivity) has a trough (peak) around 310 K.

We then asked whether there was any use for this equilibration technique other than for calculating the ECS. This question is identical to asking whether the direct effects of CO₂ are important. In section 7, we calculated the direct effect of CO₂ (right column of Figure 8) and the effect of warming (middle column of Figure 8) for all SST values from 285 to 320 K in 1-K increments. Averaging over height and SST, the direct effect of CO₂ on cloud fraction is an order of magnitude smaller than the effect of warming on cloud fraction, and the relative effects of CO₂ on tropospheric temperature and specific humidity are even smaller (see Figure 9). Nevertheless, the small direct effect on shallow clouds matches what has been reported in previous studies of global climate models, namely the lowering of the cloud heights and the decrease in their areal fraction (see Figure 10). In contrast to those small effects, the direct effect of CO₂ on net radiative cooling of the troposphere is about one third as large as the effect of warming (see Figure 9), implying a substantial direct effect on precipitation. This was confirmed in Figure 11c, where we see that the direct effect of CO₂ lowers the mean precipitation-rate increase from 3.0% K⁻¹ to 2.3% K⁻¹. Consistent with recent theoretical developments about convective available potential energy (CAPE), the direct effect of CO₂ on CAPE was found to be quite negligible (Figure 11b).

As noted in section 1, the equilibration technique described in section 3 can be adapted to any greenhouse gas or atmospheric aerosol. Furthermore, the equilibration technique can be adapted for use in a global climate model. For simplicity, consider an equinoctial aquaplanet with a 2D slab ocean (i.e., with spatially varying SST) that has an applied Q flux (a spatially varying heat source to emulate heat transport by an ocean circulation). Let us write the evolution equation for the SST as

$$C_s \frac{\partial T_s}{\partial t} = H, \quad (10)$$

where C_s is the per-area slab-ocean heat capacity and H is the sum of net downwelling surface radiative flux, turbulent enthalpy flux, and applied Q flux. Then, imagine that we have a simulation that is equilibrated over this slab ocean with a preindustrial CO₂ concentration. To map out the response of the aquaplanet to varying CO₂, we can restart a simulation with its SST pattern incremented everywhere by some ΔT_s . We then evolve the CO₂ concentration according to equation (8) and evolve the SST according to a modified

version of equation (10),

$$C_s \frac{\partial T_s}{\partial t} = H - \overline{H}, \quad (11)$$

where \overline{H} is the global mean of H . This equation allows the SST pattern to evolve while holding the mean SST fixed. As in the case of a small-domain RCE, this fixed-global-mean-SST/prognostic-CO₂ methodology eliminates the long timescale (caused by the planet’s small feedback parameter) that would otherwise dominate the approach to equilibrium in a standard slab-ocean simulation.

9. Acknowledgments

This work was supported by the U.S. Department of Energy’s Atmospheric System Research, an Office of Science, Office of Biological and Environmental Research program; Lawrence Berkeley National Laboratory is operated for the DOE by the University of California under Contract DE-AC02-05CH11231. Simulations were performed on the Lawrencium computational cluster resource provided by the IT Division at the Lawrence Berkeley National Laboratory.

10. Appendix

To easily estimate the atmospheric heat capacity C_a , let us neglect warming-induced changes in $\rho(z)$ and in the lapse rate (i.e., by assuming that the temperature change is the same at all heights). We can further simplify matters by approximating relative humidity as constant, in both height and time. Then, C_a is approximately given by

$$C_a \approx c_{pa}M_a + \frac{L^2}{R_v T_a^2} M_v, \quad (12)$$

where M_a is the mass per area of the atmosphere, M_v is mass per area of atmospheric water vapor, c_{pa} is the specific heat capacity of dry air at constant pressure, L is the specific latent enthalpy of evaporation, and R_v is the specific gas constant for water vapor. This expression for C_a is derived by taking the derivative with respect to temperature of the atmosphere’s sensible heat ($c_{pa}T_aM_a$) and latent heat (LM_v) and noting that $\partial M_a/\partial T_a = 0$ and, by Clausius-Clapeyron, $\partial M_v/\partial T_a = LM_v/R_v T_a^2$ (see also equation 13 of Cronin and Emanuel 2013). For $M_a = 10^4 \text{ kg m}^{-2}$ and a typical tropical value for M_v of 60 kg m^{-2} , both terms on the right-hand side of (12) are about $10^7 \text{ J m}^{-2} \text{ K}^{-1}$ each, so $C_a \approx 2 \times 10^7 \text{ J m}^{-2} \text{ K}^{-1}$. For $\lambda \approx -1.5 \text{ W m}^{-2} \text{ K}^{-1}$, $C_a/|\lambda|$ equals about 150 days. This is the equilibration timescale for a mixed-layer depth of zero. Each meter of slab ocean adds about 30 days to the timescale, which is calculated as the product of the specific heat capacity of liquid water times 10^3 kg m^{-2} divided by λ .

For the case of an atmosphere over an ocean with an infinite heat capacity, the response to a perturbation in either the sea-surface temperature (ΔT_s) and/or a perturbation in the atmosphere’s near-surface air temperature (ΔT_a) can be written as

$$C_a \frac{d}{dt} \Delta T_a = \chi_s \Delta T_s - \chi_a \Delta T_a, \quad (13)$$

where χ_s is the change in net upwelling surface enthalpy fluxes (sensible, latent, and radiative) per change in sea temperature, and χ_a is the change in net downwelling surface enthalpy fluxes per change in atmospheric temperature at constant surface-air relative humidity. The values of χ_s and χ_a depend on the base state and they are not exactly the same, but they are similar enough in magnitude that we can, for our purposes, approximate them by a single value χ .

To estimate χ , we can consider how the net upwelling sensible heat flux (SHF), latent heat flux (LHF), and radiative flux (RAD) change due to an increment in ocean temperature. Using a bulk aerodynamic formula for SHF and LHF, the enthalpy fluxes are:

$$\text{SHF} = C_k |u| \rho c_{pa} (T_s - T_a) \quad (14)$$

$$\text{LHF} = C_k |u| \rho L \left[q_v^*(T_s) - RH q_v^*(T_a) \right] \quad (15)$$

$$\approx C_k |u| \rho L \left[1 - RH + RH \gamma (T_s - T_a) \right] q_v^*(T_s) \quad (16)$$

$$\text{RAD} = \sigma T_s^4 - F_{\text{down}}(T_a), \quad (17)$$

where $\gamma = L/R_v T_s^2$ is the Clausius-Clapeyron rate. Taking the partial derivative with respect to T_s , we get

$$\frac{\partial \text{SHF}}{\partial T_s} = \frac{\text{SHF}}{T_s - T_a} \quad (18)$$

$$\frac{\partial \text{LHF}}{\partial T_s} = \gamma \frac{1 + \gamma RH (T_s - T_a)}{1 - RH + RH \gamma (T_s - T_a)} \text{LHF} \quad (19)$$

$$\frac{\partial \text{RAD}}{\partial T_s} = 4\sigma T_s^3. \quad (20)$$

For typical RCE values of $\text{SHF} = 10 \text{ W m}^{-2}$, $\text{LHF} = 100 \text{ W m}^{-2}$, $\gamma = 0.06 \text{ K}^{-1}$, $RH = 0.8$, $T_s - T_a = 1 \text{ K}$, and $T_s = 300 \text{ K}$, these evaluate to

$$\frac{\partial \text{SHF}}{\partial T_s} \approx 10 \text{ W m}^{-2} \text{ K}^{-1} \quad (21)$$

$$\frac{\partial \text{LHF}}{\partial T_s} \approx 25 \text{ W m}^{-2} \text{ K}^{-1} \quad (22)$$

$$\frac{\partial \text{RAD}}{\partial T_s} \approx 6 \text{ W m}^{-2} \text{ K}^{-1}. \quad (23)$$

Summing these, we get $\chi \approx 40 \text{ W m}^{-2} \text{ K}^{-1}$, which matches the value that Gill (1982) obtained for the tropics by application of the equations of Haney (1971). Writing equation (13) with $\chi_s = \chi_a = \chi$ gives equation (3).

References

- Andrews, T. and P. M. Forster, 2008: CO₂ forcing induces semi-direct effects with consequences for climate feedback interpretations. *Geophysical Research Letters*, **35** (4), L04 802.
- Andrews, T. and M. A. Ringer, 2014: Cloud feedbacks, rapid adjustments, and the forcing–response relationship in a transient CO₂ reversibility scenario. *Journal of Climate*, **27** (4), 1799–1818.
- Bretherton, C., 2007: *The Global Circulation of the Atmosphere*, chap. Challenges in numerical modeling of tropical circulations, 302–330. Princeton University Press.
- Bretherton, C. S., P. N. Blossey, and C. Stan, 2014: Cloud feedbacks on greenhouse warming in the superparameterized climate model SP-CCSM4. *Journal of Advances in Modeling Earth Systems*, **6** (4), 1185–1204.
- Caballero, R. and M. Huber, 2013: State-dependent climate sensitivity in past warm climates and its implications for future climate projections. *Proceedings of the National Academy of Sciences*, **110** (35), 14 162–14 167.
- Cess, R. D. and G. L. Potter, 1988: A methodology for understanding and intercomparing atmospheric climate feedback processes in general circulation models. *Journal of Geophysical Research: Atmospheres*, **93** (D7), 8305–8314.
- Clough, S. A., M. W. Shephard, E. J. Mlawer, J. S. Delamere, M. J. Iacono, K. Cady-Pereira, S. Boukabara, and P. D. Brown, 2005: Atmospheric radiative transfer modeling: a summary of the AER codes. *Journal of Quantitative Spectroscopy and Radiative Transfer*, **91** (2), 233–244.
- Colman, R. and B. McAvaney, 2009: Climate feedbacks under a very broad range of forcing. *Geophysical Research Letters*, **36** (1).
- Colman, R. A. and B. J. McAvaney, 2011: On tropospheric adjustment to forcing and climate feedbacks. *Climate dynamics*, **36** (9-10), 1649.
- Cronin, T. W., 2014: On the choice of average solar zenith angle. *Journal of the Atmospheric Sciences*, **71** (8), 2994–3003.
- Cronin, T. W. and K. A. Emanuel, 2013: The climate time scale in the approach to radiative-convective equilibrium. *Journal of Advances in Modeling Earth Systems*, **5** (4), 843–849.
- Cronin, T. W. and A. A. Wing, 2017: Clouds, circulation, and climate sensitivity in a radiative-convective equilibrium channel model. *Journal of Advances in Modeling Earth Systems*, **9** (8), 2883–2905.

- Dacie, S., L. Kluft, H. Schmidt, B. Stevens, S. A. Buehler, P. J. Nowack, S. Dietmüller, N. L. Abraham, and T. Birner, 2019: A 1D RCE study of factors affecting the tropical tropopause layer and surface climate. *Journal of Climate*, **32** (20), 6769–6782.
- Gill, A. E., 1982: *Atmosphere-Ocean Dynamics*, International Geophysics Series, Vol. 30. Academic Press.
- Gregory, J. and M. Webb, 2008: Tropospheric adjustment induces a cloud component in CO₂ forcing. *Journal of Climate*, **21** (1), 58–71.
- Gregory, J. M., W. J. Ingram, M. A. Palmer, G. S. Jones, P. A. Stott, R. B. Thorpe, J. A. Lowe, T. C. Johns, and K. D. Williams, 2004: A new method for diagnosing radiative forcing and climate sensitivity. *Geophysical Research Letters*, **31** (3).
- Haney, R. L., 1971: Surface thermal boundary condition for ocean circulation models. *Journal of Physical Oceanography*, **1** (4), 241–248.
- Hansen, J., M. Sato, R. Ruedy, L. Nazarenko, A. Lacis, G. Schmidt, G. Russell, I. Aleinov, M. Bauer, S. Bauer, et al., 2005: Efficacy of climate forcings. *Journal of Geophysical Research*, **110** (D18), D18104.
- Held, I. M. and B. J. Soden, 2006: Robust responses of the hydrological cycle to global warming. *Journal of Climate*, **19**, 5686–5699.
- Iacono, M. J., J. S. Delamere, E. J. Mlawer, M. W. Shephard, S. A. Clough, and W. D. Collins, 2008: Radiative forcing by long-lived greenhouse gases: Calculations with the AER radiative transfer models. *Journal of Geophysical Research*, **113** (D13).
- Kamae, Y. and M. Watanabe, 2013: Tropospheric adjustment to increasing CO₂: its timescale and the role of land–sea contrast. *Climate Dynamics*, **41** (11-12), 3007–3024.
- Kamae, Y., M. Watanabe, T. Ogura, M. Yoshimori, and H. Shiogama, 2015: Rapid adjustments of cloud and hydrological cycle to increasing CO₂: a review. *Current Climate Change Reports*, **1** (2), 103–113.
- Khairoutdinov, M. F. and C.-E. Yang, 2013: Cloud-resolving modelling of aerosol indirect effects in idealised radiative-convective equilibrium with interactive and fixed sea surface temperature. *Atmospheric Chemistry and Physics*, **13** (8), 4133–4144.
- Kluft, L., S. Dacie, S. A. Buehler, H. Schmidt, and B. Stevens, 2019: Re-examining the first climate models: Climate sensitivity of a modern radiative-convective equilibrium model. *Journal of Climate*, **32** (23), 8111–8125.
- Kopp, G., 2016: Magnitudes and timescales of total solar irradiance variability. *Journal of Space Weather and Space Climate*, **6**, A30.

- Krueger, S., Q. Fu, K. Liou, and H. Chin, 1995: Improvements of an ice-phase microphysics parameterization for use in numerical simulations of tropical convection. *Journal of Applied Meteorology*, **34** (1), 281–287.
- Lambert, F. H. and M. J. Webb, 2008: Dependency of global mean precipitation on surface temperature. *Geophysical Research Letters*, **35** (16).
- Leconte, J., F. Forget, B. Charnay, R. Wordsworth, and A. Pottier, 2013: Increased insolation threshold for runaway greenhouse processes on Earth-like planets. *Nature*, **504** (7479), 268.
- Lin, Y., R. Farley, and H. Orville, 1983: Bulk parameterization of the snow field in a cloud model. *Journal of Applied Meteorology*, **22** (6), 1065–1092.
- Lord, S., H. Willoughby, and J. Piotrowicz, 1984: Role of a parameterized ice-phase microphysics in an axisymmetric, nonhydrostatic tropical cyclone model. *Journal of the Atmospheric Sciences*, **41** (19), 2836–2848.
- Manabe, S. and R. T. Wetherald, 1967: Thermal equilibrium of the atmosphere with a given distribution of relative humidity. *Journal of the Atmospheric Sciences*, **24** (3), 241–259.
- Meraner, K., T. Mauritsen, and A. Voigt, 2013: Robust increase in equilibrium climate sensitivity under global warming. *Geophysical Research Letters*, **40** (22), 5944–5948.
- Mitchell, J. F. B., C. A. Wilson, and W. M. Cunnington, 1987: On CO₂ climate sensitivity and model dependence of results. *Quarterly Journal of the Royal Meteorological Society*, **113** (475), 293–322.
- Muller, C. J., P. A. O’Gorman, and L. E. Back, 2011: Intensification of precipitation extremes with warming in a cloud-resolving model. *Journal of Climate*, **24**, 2784–2800.
- Newell, R. E. and T. G. Dopplick, 1970: Effect of changing CO₂ concentration on radiative heating rates. *Journal of Applied Meteorology*, **9** (6), 958–959.
- O’Gorman, P. A., R. P. Allan, M. P. Byrne, and M. Previdi, 2012: Energetic constraints on precipitation under climate change. *Surveys in Geophysics*, **33** (3-4), 585–608.
- Popp, M., H. Schmidt, and J. Marotzke, 2016: Transition to a moist greenhouse with CO₂ and solar forcing. *Nature Communications*, **7**, 10627–.
- Romps, D. M., 2008: The dry-entropy budget of a moist atmosphere. *Journal of the Atmospheric Sciences*, **65** (12), 3779–3799.
- Romps, D. M., 2011: Response of tropical precipitation to global warming. *Journal of the Atmospheric Sciences*, **68** (1), 123–138.
- Romps, D. M., 2016: Clausius-Clapeyron scaling of CAPE from analytical solutions to RCE. *Journal of the Atmospheric Sciences*, **73** (9), 3719–3737.

- Romps, D. M., 2019: Evaluating the future of lightning in cloud-resolving models. *Geophysical Research Letters*, **46**, 14,863–14,871.
- Russell, G. L., A. A. Lacis, D. H. Rind, C. Colose, and R. F. Opstbaum, 2013: Fast atmosphere-ocean model runs with large changes in CO₂. *Geophysical Research Letters*, **40** (21), 5787–5792.
- Schlesinger, M. E., 1986: Equilibrium and transient climatic warming induced by increased atmospheric CO₂. *Climate Dynamics*, **1** (1), 35–51.
- Seeley, J. T., N. Jeevanjee, W. Langhans, and D. M. Romps, 2019: Formation of tropical anvil clouds by slow evaporation. *Geophysical Research Letters*, **46**, 492–501.
- Seeley, J. T. and D. M. Romps, 2016: Why does tropical convective available potential energy (CAPE) increase with warming? *Geophysical Research Letters*, **42** (23), 10 429–10 437.
- Sherwood, S. C., S. Bony, O. Boucher, C. Bretherton, P. M. Forster, J. M. Gregory, and B. Stevens, 2015: Adjustments in the forcing-feedback framework for understanding climate change. *Bulletin of the American Meteorological Society*, **96** (2), 217–228.
- Singh, M. S. and P. A. O’Gorman, 2013: Influence of entrainment on the thermal stratification in simulations of radiative-convective equilibrium. *Geophysical Research Letters*, **40** (16), 4398–4403.
- Singh, M. S. and P. A. O’Gorman, 2015: Increase in moist-convective updraft velocities with warming in radiative-convective equilibrium. *Quarterly Journal of the Royal Meteorological Society*, **141** (692), 2828–2838.
- Stephens, G. and T. Ellis, 2008: Controls of global-mean precipitation increases in global warming GCM experiments. *Journal of Climate*, **21**, 6141–6155.
- Tian, B., G. Zhang, and V. Ramanathan, 2001: Heat balance in the Pacific warm pool atmosphere during TOGA COARE and CEPEX. *Journal of Climate*, **14** (8), 1881–1893.
- Wolf, E. T., J. Haqq-Misra, and O. B. Toon, 2018: Evaluating climate sensitivity to CO₂ across Earth’s history. *Journal of Geophysical Research: Atmospheres*, **123** (21), 11–861.
- Wolf, E. T. and O. B. Toon, 2015: The evolution of habitable climates under the brightening Sun. *Journal of Geophysical Research: Atmospheres*, **120** (12), 5775–5794.
- Wyant, M. C., C. S. Bretherton, P. N. Blossey, and M. Khairoutdinov, 2012: Fast cloud adjustment to increasing CO₂ in a superparameterized climate model. *Journal of Advances in Modeling Earth Systems*, **4** (2).
- Zelinka, M. D., S. A. Klein, K. E. Taylor, T. Andrews, M. J. Webb, J. M. Gregory, and P. M. Forster, 2013: Contributions of different cloud types to feedbacks and rapid adjustments in CMIP5. *Journal of Climate*, **26** (14), 5007–5027.